Photoionization pathways and free electrons in UV-MALDI

Richard Knochenmuss
Novartis Institutes for Biomedical Research
4002 Basel, Switzerland
email: richard.knochenmuss@pharma.novartis.com
tel: ++41 61 324 4541
fax: ++41 61 324 8828

Abstract

The recently developed comprehensive model for UV-MALDI (*J. Mass Spectrom.* **2002**, *37*, 867-877, *Anal. Chem.* **2003**, *75*, 219) is applied to questions regarding photoionization pathways and electron production. Direct 2-photon ionization of matrix coordinated with analyte is possible under some circumstances (*J. Mass Spectrom.* **2002**, *37*, 1131-1140), and is added to the model. Only when analyte is present in atypically large mole ratios is this effect able to contribute significantly to ion production. Since matrix is normally present in large excess, exciton pooling remains dominant. The interfacial layer of thin samples on a metal substrate may also be ionizable in a direct 2-photon process. A mechanism is proposed, and the correspondingly modified model gives excellent agreement with electron emission data. Capture or escape of low energy electrons is also examined. From measured cross sections, the mean free path for MALDI electrons in solid matrix is on the order of 10 nm. Below this depth, any electrons generated are captured to form negative ions, only the surface layer emits electrons. The model successfully reproduces the electron yield of thick samples, but emission is limited by surface charging. This charging effect is illustrated by molecular dynamics calculations.

Introduction

The production of charged species in UV-MALDI has been a topic of ongoing interest.(1-8) Understanding of ionization mechanisms is clearly a prerequisite for rational, directed development of the method, as well as interpreting and quantifying the data.

At least for the matrix 2,5 dihydroxybenzoic acid, considerable progress has recently been made. A comprehensive, quantitive model for UV-MALDI ion generation in this matrix has been presented.(1, 2) It has proven highly successful when tested against wide-ranging experimental results. The primary photochemical events included in the model are laser excitation of individual matrix molecules, and exciton pooling events. In the latter, two nearby excited matrix molecules can redistribute their energy to an isoenergetic state in which energy is concentrated on one molecule. This is a well-known phenomenon in condensed aromatic systems,(9) and was found to be the main pathway leading to ions for the matrix 2,5 dihydroxybenzoic acid (DHB).

As proposed in detail by Knochenmuss et al.,(10) and supported by more recent evidence,(3, 11) analyte ionization in MALDI is believed to be thermodynamically determined, as the result of extensive secondary ion-molecule reactions in the plume. Primary matrix ions are converted to the most favorable secondary products, including analyte ions, which are then observed at the detector. These reactions are not specific to any particular matrix, and the concept has been shown to have quantitative or semi-quantitative predicitve ability for many matrices and analytes.

In the present study, we consider the possible roles of ionization pathways which were not included in the original model. The first of these was suggested by the work of the Kinsel group(12-14) in which it was found that matrix-analyte complexes could, in some circumstances, exhibit significantly reduced ionization potentials (IPs) compared to the individual uncomplexed molecules. This was experimentally demonstrated in detail for DHB-proline complexes, and the mechanism of IP reduction was theoretically investigated. Charge transfer via hydrogen bonds was found to decrease the IP of the complexed matrix from 8.05 eV to 7.0 eV, well below the 2-photon energy of the nitrogen laser (7.36 eV). The Kinsel group has found considerable evidence that similar IP reductions occur in other matrix-analyte complexes.(13, 14) As a result of these findings, it is important to investigate what part of the observed MALDI ion current might be a result of 2-photon ionization of matrix complexed with analyte in the solid sample.

Another process which was not included in refs. (1, 2) involves the sample substrate. The magnitude of electron emission from MALDI samples can vary on metallic vs. insulating substrates. As detected by capture of electrons by neutral SF_6, thin samples on a metal substrate yielded more photoelectrons than thick samples or samples on an

insulating substrate.(15, 16) This suggests that the interfacial matrix layer on a metal might be a significant ion source, especially if the process is sufficiently low in energy to be achieved with one laser photon.(15)

Electrons may be important for influencing the relative yield of ions with charge states larger than one. These were considered to be an important indicator of MALDI mechanisms by some workers,(6) who proposed that free electrons neutralize most of the higher charge states. However, others concluded that the charge state distribution is determined more by the energetics of ion-molecule reactions that occur in the plume.(10)

The data pertaining to these mechanisms will be evaluated in comparison with the existing model. This leads to new understanding of certain special cases in MALDI, but shows that the dominant processes are usually those already present in the prior model. It is also found that thin sample photoemission is a 2-photon process, and that only the upper few nanometers of a "thick" sample yield free electrons.

Matrix-Analyte Cluster Photoionization

As noted above, appropriately coordinated matrix-analyte complexes may exhibit very low ionization potentials, enabling 2-photon ionization by N_2 (337 nm) or tripled Nd:YAG (355 nm) lasers.(12) Such ions have been calculated to undergo barrierless secondary intra-cluster proton transfer from matrix to analyte, leading to the commonly observed protonated analyte species.(12) This can be described as primary matrix ionization followed by reaction with neutral analyte, but the primary step is enabled by analyte, blurring the distinction between primary and secondary reactions.

Two-photon cluster photoionization cannot be active for all analytes and matrices, since it depends on particularly favorable matrix-analyte coordination. However, it may not be rare, so it is important to consider to what extent it can contribute for appropriate matrix-analyte systems. To evaluate this, new terms were added to the rate equation model of Refs. (1, 2). For analyte A and matrix M, the process is:

$$M^*A \xrightarrow[h\nu]{} M\,A^+$$

$$d[A^+]/dt = \text{previous} + \sigma_{1\text{-}I}\, I\, D\, C\, [A][M^*]$$

Where M* is singly excited matrix, I is the laser intensity, $\sigma_{1\text{-}I}$ is the cross section for S_1 to ion photoionization of the M-A complex, and C is a molecular surface area scale factor. The latter accounts for the increased probability that a large analyte will be near an excited matrix molecule and was described in the original model.(1) D is the desorption pressure ratio scale factor, which accounts for decreasing collision rates as the plume

expands, as also described in the original model.(1) Corresponding terms must, of course, be added to the rate expressions for M, M*, and A.

The only unknown parameter in this addition to the model is the photoionization cross section, $\sigma_{1\text{-}I}$. An upper limit can, however, be readily estimated. A consistent feature of all matrix-analyte cluster photoionization studies to date is the observation of quadratic dependencies on the excitation laser intensity.(12-14) This has been important in establishing characteristics of these clusters. This has the useful consequence that it limits the maximum value of $\sigma_{1\text{-}I}$ to the same magnitude as the cross section for absorption from the ground state to the first excited state, $\sigma_{0\text{-}1}$. If this were not so, then the 0-1 step would be rate limiting for the 2-photon process, and the power dependence would approach linearity. An exponent of 2 for the power dependence would not be reached.

Simulations were therefore carried out assuming $\sigma_{1\text{-}I} = \sigma_{0\text{-}1}$. All other matrix parameters were as in refs (1, 2), for DHB, and a laser wavelength of 355 nm. The results are shown in Fig. 1. At analyte concentrations typical of most routine measurements (1% or less) there is little difference between the analyte ion yields with and without direct photoionization of MA clusters. Only at atypically high analyte concentrations is a significant difference observed. This increases siowly at higher fluences, but cluster photoionization never becomes a dominant ionization pathway for fluences less than 50% higher than the threshold.

Figure 1 here

The dominant analyte ion generation pathway is the 2-step process previously modelled: primary matrix ions are generated by exciton pooling processes, and these react secondarily with neutral analyte. Two values of the exoergicity of the matrix ion + analyte charge transfer reaction were used for the calculations in Fig. 1. The first value, -150 kJ/mol, corresponds to proton transfer from matrix to typical proteins or peptides. The reaction is rapid, with a small activation energy. In this case, it is not surprising that cluster photoionization is a small large contributor, since the 2-step pathway is efficient. More interesting is the observation that the same conclusion holds with a low value for the reaction exoergicity of -30 kJ/mol. This corresponds to cationization reactions with metal ions. In this case the matrix-analyte secondary reaction is slowed by a significant activation barrier, but is still fast enough that cluster photoionization remains a minor effect.

Photoelectron emission at the sample-metal interface

Recent studies have shown a marked difference in MALDI spectra as a function of

sample substrate.(15-18) This has been attributed to photoelectron emission at the interface between matrix and metal substrates.(15-17) This concept has not been fully explored in the UV-MALDI context and deserves further consideration.

Figure 2 here

Figure 2 schematically illustrates the situation when a DHB matrix molecule is deposited on a metal substrate. The IP of free a DHB molecule (IP_{free}) is 8.054 eV,(19) approximately the energy require to lift an electron out of the highest occupied molecular orbital (HOMO). The first excited state, obtained by promoting an electron from the HOMO to the lowest unoccupied molecular orbital (LUMO), is 3.466 eV above this, or 4.588 eV below the vacuum level. This lies in the range of the Fermi level of typical substrates like stainless steel or gold, at 4.5-5.1 eV below the vacuum level. This energy is also known as the work function of the metal, ϕ. As a result of adsorbate-molecule interactions such as exchange or Coulomb interactions, metal and matrix orbitals are mixed, as shown in the center of the diagrams. The degree of splitting is determined by the strength of the interaction and is often of the order of 1 eV.(20)

The two cases relevant here are shown in Fig. 2. If the orbitals resulting from surface interactions with the matrix LUMO remain above the metal Fermi level, then they do not become populated, as shown in (a). However, the HOMO of the adsorbed DHB is raised in energy by the interaction potential of that orbital with the metal conduction band. The adsorbed IP (IP_{ads}) is then $IP_{free} - V_{surf\text{-}DHB}$. If the interaction is larger than 0.54 eV, the adsorbed molecule can be ionized by two photons of 337 nm (7.36 eV). If it is larger than 1 eV, two 355 nm photons (7.02 eV) are also sufficient.

In case (b), the upper mixed orbitals fall below the Fermi level, and become populated from the bulk metal, creating a new HOMO at considerably higher energy than in (a). A net dipole develops between the metal and the first matrix layer. It should be noted that IP_{ads} remains too large for one-photon ionization, since the new HOMO lies below the Fermi level. However, it is clearly possible for two 355 or 337 nm photons to sequentially ionize interfacial molecues.

At this point it is perhaps useful to note that, while energetically feasible, two 355 or 337 nm photons will not efficiently ionize the bare metal surface at MALDI-like laser intensities. There are three reasons for this. First, most metals will reflect these wavelengths to a high degree. Gold has a higher absorptivity in the near-UV than stainless steel, but still reflects considerably. Second, efficient 2-photon ionization requires a resonant intermediate state with a significant lifetime, so that it is not necessary for both photons to be incident at the same time. Only at high intensities is a

simultaneous 2-photon process efficient. In the relevant metals, the top of the conduction band lies too low for this. Third, even if a resonant intermediate state is accessible, electronic excitations in the conduction bands of metals are very short-lived, so this case is nearly the same as if no intermediate state is available.

Via resonant absorption to the illustrated intermediate excited states, 2-photon ionization in case (a) will obviously be efficient. Less obviously, in case (b) it is also expected to be facile. The manifold of higher electronic excited states is fairly dense, an allowed transition to a resonant intermediate state below the IP is highly likely. It is even more likely than suggested by Fig. 2, since the vibrational manifolds of each electronic state span substantial energy ranges. These are then also broadened by intermolecular interactions in the solid state. The upper part of the figure will be effectively filled by DHB states.

The models of Fig. 2 for surface matrix ionization can be readily tested. In ref. (15) the yield of photoelectrons from a thin DHB sample on a metal substrate versus laser pulse energy was reported (Fig. 4a of Ref (15)). If these electrons are due to a one-photon process, this curve should exhibit a linear form. Instead one notes a distinct curvature that is nevertheless less than quadratic. It seems plausible that surface photoionization acts in conjunction with pooling mechanisms to produce a composite curve.

A system of differential equations including the mechanisms of Fig. 2(a) can be readily obtained from the exisiting MALDI model, with two simplifying changes. First, only 2 neutral states are relevant, the S_0 and the S_1. The original model needed also to consider the Sn, at the 2-photon energy, but below the IP. Second, the plume expansion can be neglected, since photoemission of electrons can take place only during the laser pulse, before the expansion has a significant effect. Pooling of two S_1 excited states must be retained since this can now generate ions directly. The differential equations are then:

$$\frac{d[S_0]}{dt} = -I(t)\sigma_{01}(\lambda)[S_0] + \frac{[S_1]}{\tau_1} + k_{11}[S_1]^2$$

$$\frac{d[S_1]}{dt} = I(t)\sigma_{01}(\lambda)[S_0] - \frac{[S_1]}{\tau_1} - I(t)\sigma_{1-I}(\lambda)[S_1] - 2k_{11}[S_1]^2$$

$$\frac{d[S_n]}{dt} = I(t)\sigma_{1-I}(\lambda)[S_1] + k_{11}[S_1]^2$$

These equations were integrated numerically with 5-th order Runge-Kutta methods, assuming a 5 ns, 355 nm gaussian laser pulse. Using the previously determined parameters for DHB,(1) excellent agreement with the electron emission data is immediately obtained, as seen in Fig. 3.

Figure 3 here

This represents a sequential two-photon ionization process in parallel with $S_1 + S_1$ pooling. No fitting of parameters was performed. It was only necessary to linearly scale the experimental data since absolute yields and laser fluences were not reported. The laser spot size was taken to be 0.01 cm^2, from experience with the instrument.

Since the MALDI model is successful in this modified form in describing electron emission from metal surfaces, it should be capable of treating the same problem on a insulating surface (fig. 4b in ref (15)), where no such charge transfer effects are expected. The data are compared with calculation in Fig. 4. The dashed curve represents the experimental results with the assumption that the laser spot size was the same in both figs 4a and 4b of Ref (15). Clearly the calculated and measured ionization thresholds are not the same. Since the calculated result was previously shown to give an accurate threshold,(1) it is concluded that the experimental fluence values were not the same as in Fig. 3. Aligning the threholds by laterally shifting the experimental curve leads to excellent agreement, at least up to the point where the curve flattens.

Figure 4 here

In Fig. 4 the theoretical curve represents the yield from the top layer of a DHB sample, and not the yield integrated over the thickness of the sample, as would be necessary to calculate the total MALDI ion yield. (1) This is the appropriate comparison because electrons are captured in deeper layers, as discussed next.

Electron escape and charging of the MALDI sample surface

The electron capture cross section of DHB has been estimated by Asfandiarov, et al.(21) At typical solid densities, this corresponds to a mean free path on the order of 10-50 nm. This then, is the scale corresponding to “thin” with respect to substrate-related photoelectron emission, as in Fig. 3. Any sample region thicker than a few tens of nm will be too thick to emit photoelectrons from the interior, and corresponds instead to Fig. 4.

Because of the typical electron capture length, photoelectrons will always be emitted from the surface of a sample, so there is no genuinely “electron free” MALDI, even if the sample is thick or on an insulating substrate.(17) The total electron yield of a thick sample is closely connected to the flattening of the curve in Fig 4. At the top of an irradiated

sample, ionization leads to free electrons, some of which escape. The bulk of the sample retains charge neutrality, but the surface becomes postively charged. This is illustrated in Fig. 5, for a molecular dynamics simulation of a DHB sample irradiated by a 355 nm, 30 ps laser pulse.

Figure 5 here

The details of this calculation will be presented elsewhere, the key result here is the marked positively charged layer extending to about 20 nm below the surface. In the simulation shown, the layer generates an electric field on the order of up to 10^8 V/m. Typical MALDI electron energies are 1-2 eV,(21) corresponding to a distance from the surface of as little as 10^{-8} m, or 10 nm. Clearly, electrons will return to the surface rather than escape to be detected under such conditions.

This explains the sudden flattening of the experimental electron emission data in Fig. 4. Electrons are emitted from the surface layer during the laser pulse, until the surface charge becomes so large that they cannot escape. Obviously, this will always occur at the same surface charge density, resulting in the flat top, and sharp corner in the data.

Conclusions

The UV-MALDI model of refs (1, 2) has been extended to evaluate possible ionization mechanisms involving 2-photon ionization. These mechanisms are the result of matrix interactions either with analytes or with metal substrates.

Direct photoionization of matrix-analyte complexes may play a role in UV-MALDI, for appropriate matrix-analyte pairs. It does not appear to make a significant contribution to the total ion current unless the matrix:analyte ratio is atypically low (e.g. 10:1). Such ratios may, however, be of interest in practice, since they can lead to a very useful suppression of matrix ions.(2, 22) The extra analyte signal obtainable by this mechanism then increases the likelihood of achieving the desired matrix suppression and obtaining an uncluttered mass spectrum.

Metal substrates can interact with adsorbed matrix to enable 2-photon ionization of the surface matrix layer with the usual lasers. However, this is only of importance for sample regions which are thinner than a few 10s of nm, since otherwise the electrons are captured by matrix in overlying layers. Since this mechanism is limited to the interfacial layer, it has little effect on analyte ion generation efficacy in the rest of the sample. However, in some fortuitous cases of optimally thin samples, the electrons generated may help reduce any multiply charged analyted to a lower charge state.(6)

The appropriately modified MALDI model gives excellent agreement with the electron emission data for matrix on metal substrates, using the same matrix parameters as previously determined for bulk matrix.

The MALDI model also reproduces the electron emission data for thick samples, up to the plateau. Above this point, MD simulations and physical considerations point to a surface charging phenomenon. This surface charge limits the electron emission to a maximum value, regardless of further increases in laser intensity.

Acknowlegments
The author thanks Leonid Zhigilei for software, assistance and advice regarding the molecular dynamics calculations.

Literature Cited

(1) Knochenmuss, R. *J. Mass Spectrom.* **2002,** *37*, 867-877.
(2) Knochenmuss, R. *Anal. Chem.* **2003,** *75*, 2199.
(3) Knochenmuss, R.; Zenobi, R. *Chem. Rev.* **2002,** *103*, 441-452.
(4) Zenobi, R.; Knochenmuss, R. *Mass Spectrom. Rev.* **1998,** *17*, 337.
(5) Krüger, R.; Pfenninger, A.; Fournier, I.; Glückmann, M.; Karas, M. *Anal. Chem.* **2001,** *73*.
(6) Karas, M.; Glückmann, M.; Schäfer, J. *J. Mass Spectrom.* **2000,** *35*, 1-12.
(7) Livadaris, V.; Blais, J.-C.; Tabet, J.-C. *Eur. J. Mass Spectrom.* **2000,** *6*, 409-413.
(8) Fournier, I.; Brunot, A.; Tabet, J.-C.; Bolbach, G. *Int. J. Mass Spectrom.* **2002,** *213*, 203-215.
(9) Birks, J. B. *Photophysics of Aromatic Compounds*; Wiley Interscience: London, 1970.
(10) Knochenmuss, R.; Stortelder, A.; Breuker, K.; Zenobi, R. *J. Mass Spectrom.* **2000,** *35*, 1237-1245.
(11) Breuker, K.; Knochenmuss, R.; Zhang, J.; Stortelder, A.; Zenobi, R. *Int. J. Mass Spectrom.* **2003,** *226*, 211-222.
(12) Kinsel, G.; Knochenmuss, R.; Setz, P.; Land, C. M.; Goh, S.-K.; Archibong, E. F.; Hardesty, J. H.; Marynik, D. *J. Mass Spectrom.* **2002,** *37*, 1131-1140.
(13) Land, C. M.; Kinsel, G. R. *J. Am. Soc. Mass Spectrom.* **2001,** *12*, 726-731.
(14) Land, C. M.; Kinsel, G. R. *J. Am. Soc. Mass. Spectrom.* **1998,** *9*, 1060-1067.
(15) Frankevich, V.; Zhang, J.; Friess, S. D.; Dashtiev, M.; Zenobi, R. *Anal. Chem.* **2003**.
(16) Frankevich, V.; Knochenmuss, R.; Zenobi, R. *Int. J. Mass Spectrom.* **2002,** *220*, 11-19.
(17) Frankevich, V.; Zhang, J.; Dashtiev, M.; Zenobi, R. *Rapid Comm. Mass Spectrom.* **2003,** *17*, 2343-2348.
(18) Gorshkov, M. V.; Frankevich, V. E.; Zenobi, R. *Eur. J. Mass Spectrom.* **2002,** *8*, 67 - 69.
(19) Karbach, V.; Knochenmuss, R. *Rapid Commun. Mass Spectrom.* **1998,** *12*, 968-974.
(20) Lyons, L. In *Physics and Chemistry of the Organic Solid State*; Fox, D., Labes, M. M., Weissberger, A., Eds.; Interscience: New York, 1963; Vol. 1, pp 745-809.
(21) Asfandiarov, N. L.; Pshenichnyuk, S. A.; Forkin, A. I.; Lukin, V. G.; Fal'ko, V. S. *Rapid Commun. Mass Spectrom.* **2002,** *16*, 1760-1765.
(22) Knochenmuss, R.; Dubois, F.; Dale, M. J.; Zenobi, R. *Rapid Commun. Mass Spectrom.* **1996,** *10*, 871-877.

Figure Captions

Figure 1. Ion yields for analyte in DHB matrix as a function of laser fluence and analyte mole fraction in the sample. The solid lines were calculated including direct photoionization of matrix-analyte clusters, as described in the text. The dashed lines are without. The laser wavelength was 355 nm, with a 5 ns pulse width. The analyte molecular weight was 1000 Da, and the charge transfer reaction ΔG with matrix -150 or -30 kJ/mol.

Figure 2. Schematic representation of effects that may occur upon adsorption of a DHB molecule on a metallic substrate. The free metal is on the left, and free matrix on the right. The IP of free a DHB molecule (IPfree) is 8.054 eV,(19) and the first excited state is 3.466 eV above this, or 4.588 eV below the vacuum level (steel vs. gold). The work function of the metal, ϕ, is 4.5-5.1 eV below the vacuum level. Interaction of DHB orbitals with filled or emtpy conduction band orbitals can lead to either (a) a reduction of the adsorbed IP (IPads) by the interaction energy of the DHB HOMO, or (b) a reduction of IPads by filling of a LUMO-derived orbital which drops below the Fermi level. In this case a surface dipole also develops due to charge transfer from metal to adsorbate.

Figure 3. Electron emission vs. laser fluence for a "thin" DHB sample on a metal substrate. The calculated curve is described in the text, and includes sequential 2-phton ionization as well as pooling of singly excited matrix. The matrix parameters were as in Ref. (1), no fitting was performed. The data is adapted from Ref. (15).

Figure 4. Electron emission vs. laser fluence for a "thick" DHB sample, or any DHB sample on a non-metallic substrate. The calculated curve represents the full model of Ref. (1), no fitting was performed. The data is adapted from Ref. (15). The dashed data trace assumes the same horizontal axis scaling as in Fig. 3. Since the measured threshold for DHB was well reproduced in Ref. (1), the solid data trace has been shifted to align the thresholds.

Figure 5. Transverse snapshot of a molecular dynamics simulation of a DHB MALDI sample, at 350 ps. A spatially uniform 355 nm, 30 ps FWHM, temporally Gaussian laser pulse was incident from the right, centered at 35 ps. Distances are in Angstrom, the top of the sample was initially at zero. The upper panel shows all molecules, while the lower panel shows only ions. Positive ions are represented as red crosses, negative ions as blue diamonds. Note the pronounced positively charged layer at the surface, due to escape of electrons. Deeper in the sample, electrons are captured by neutral matrix before they escape, retaining approximate charge neutrality.

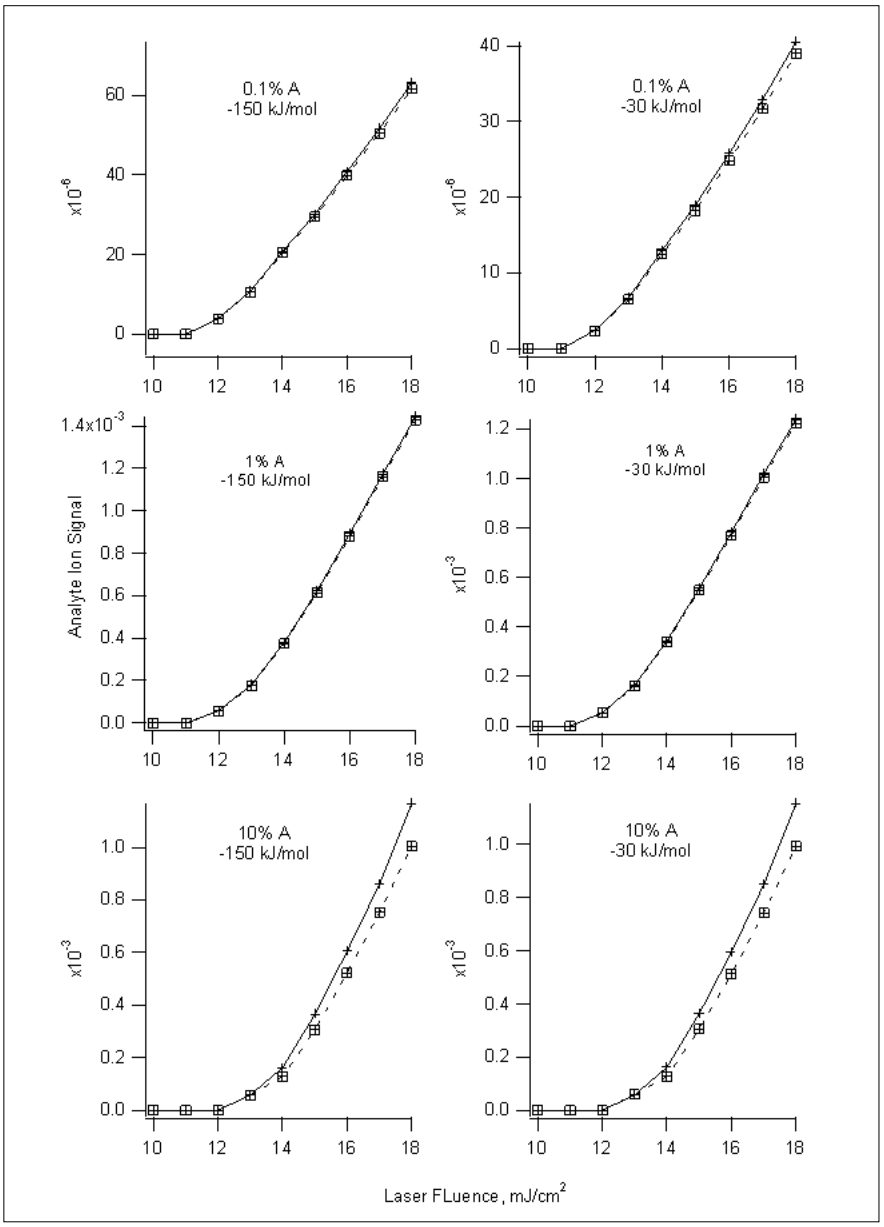
0.1% A
-150 kJ/mol
0.1% A
-30 kJ/mol
1% A
-150 kJ/mol
1% A
-30 kJ/mol
10% A
-150 kJ/mol
10% A
-30 kJ/mol
Analyte Ion Signal
Laser FLuence, mJ/cm2

Figure 1

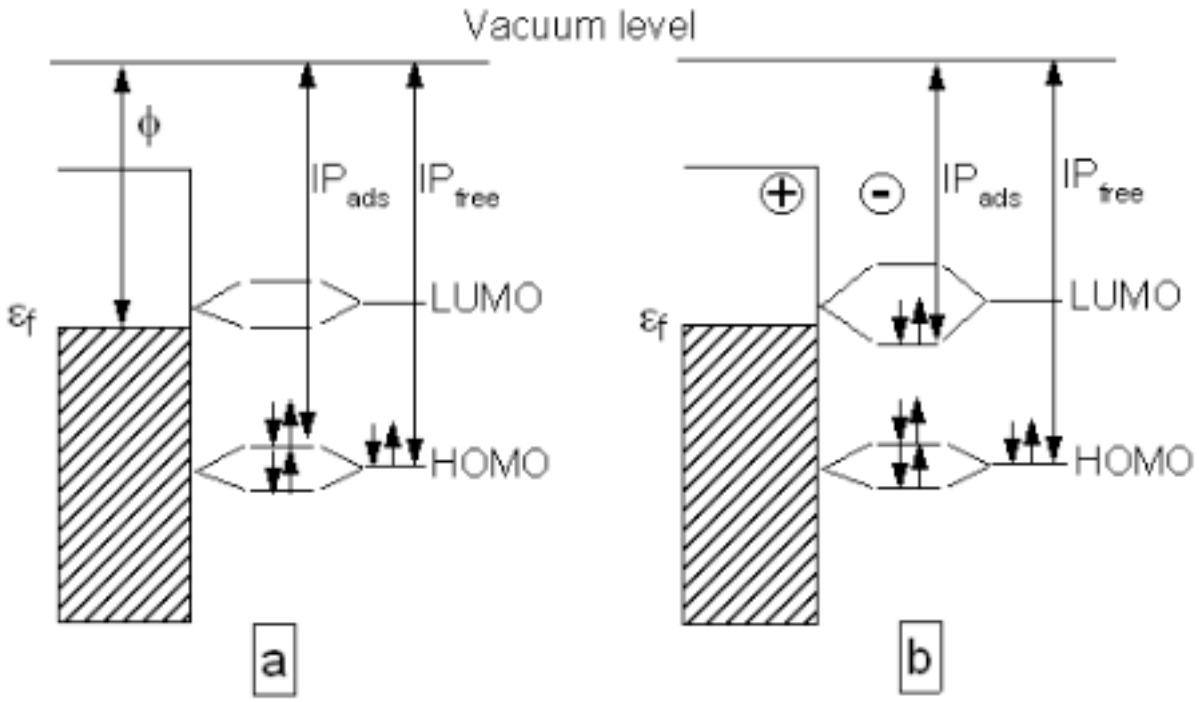
Vacuum level
ϕ
IP ads
IP free
LUMO
HOMO
εf
a
+
-
IP ads
IP free
LUMO
HOMO
εf
b

Figure 2

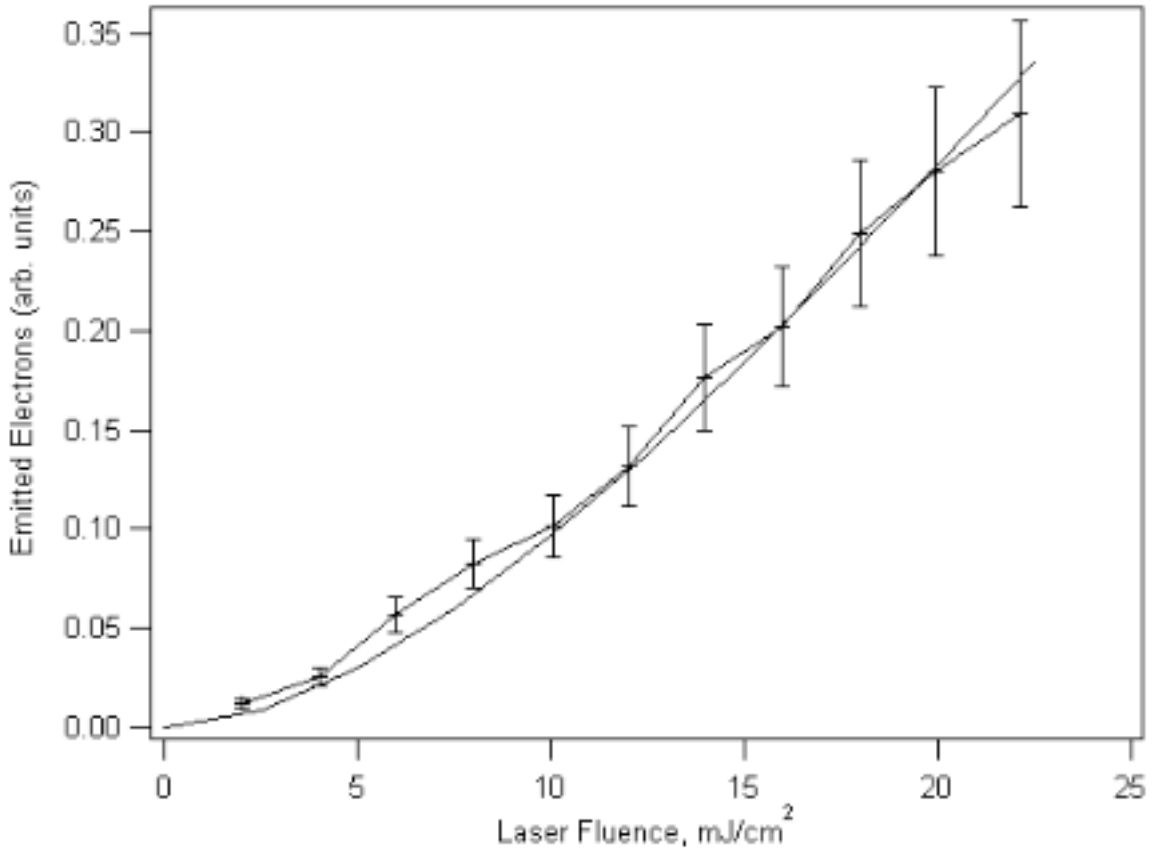
Emitted Electrons (arb. units)
0.35
0.30
0.25
0.20
0.15
0.10
0.05
0.00
0
5
10
15
20
25
Laser Fluence, mJ/cm2

Figure 3

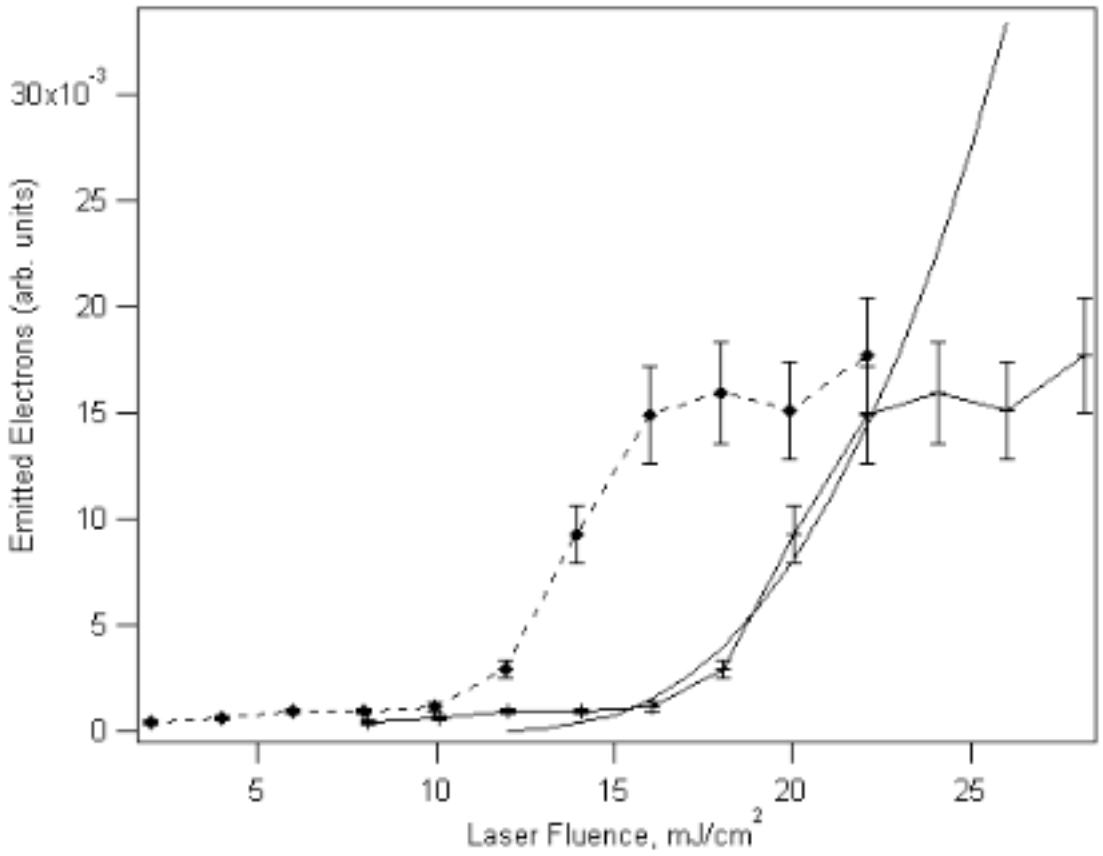
30x10^-3
25
20
15
10
5
0
Emitted Electrons (arb. units)
5
10
15
20
25
Laser Fluence, mJ/cm^2

Figure 4

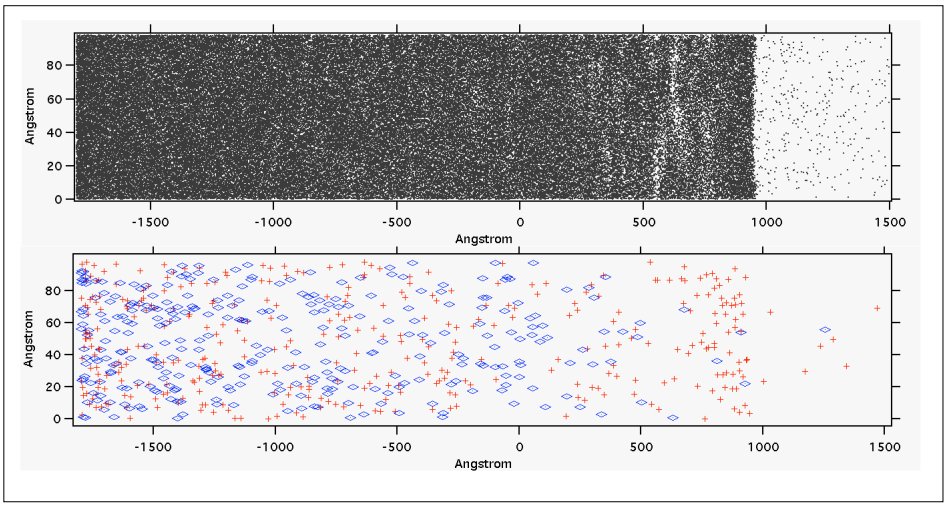
Angstrom
80
60
40
20
0
-1500
-1000
-500
0
500
1000
1500
Angstrom
Angstrom
80
60
40
20
0
-1500
-1000
-500
0
500
1000
1500
Angstrom

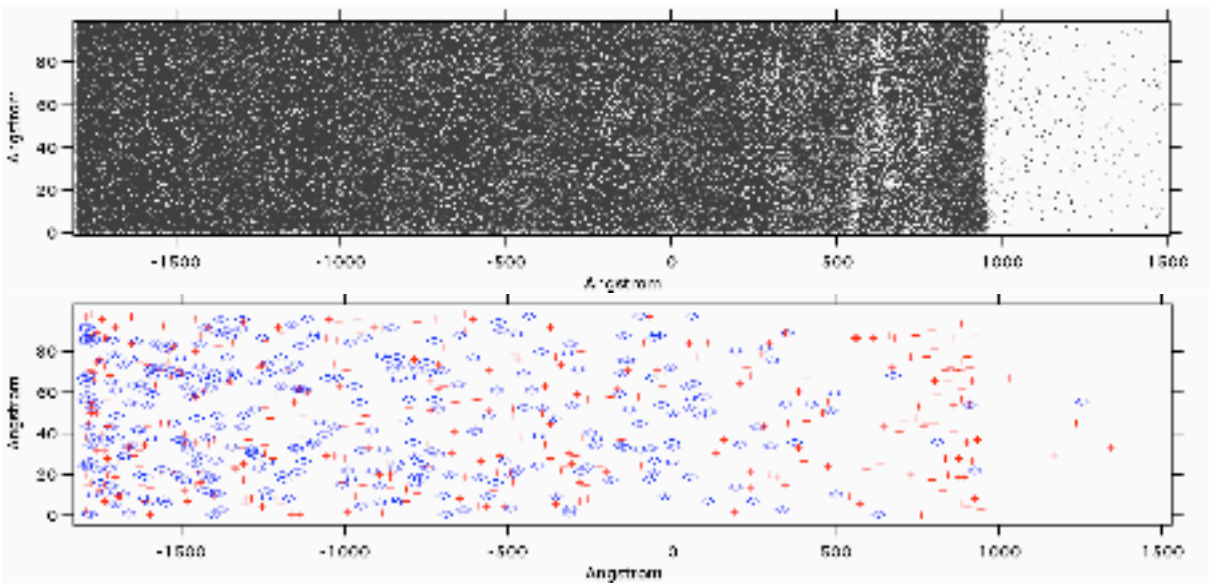
80
60
40
20
0
-1500
-1000
-500
0
500
1000
1500
Angstrom
Angstrom
80
60
40
20
0
-1500
-1000
-500
0
500
1000
1500
Angstrom

Figure 5